Published in final edited form as:
Nat Metab. 2019 September ; 1(9): 899–911. doi:10.1038/s42255-019-0109-9.

Spatial sorting enables comprehensive characterization of liver zonation

Shani Ben-Moshe[#1], **Yonatan Shapira**[#1], **Andreas E. Moor**[1,2], **Rita Manco**[1], **Tamar Veg**[1], **Keren Bahar Halpern**[1], **Shalev Itzkovitz**[1,*]

[1]Department of Molecular Cell Biology, Weizmann Institute of Science, 234 Herzl St., Rehovot, Israel 7610001

[#] These authors contributed equally to this work.

Abstract

The mammalian liver is composed of repeating hexagonal units termed lobules. Spatially resolved single-cell transcriptomics revealed that about half of hepatocyte genes are differentially expressed across the lobule, yet technical limitations impeded reconstructing similar global spatial maps of other hepatocyte features. Here, we show how zonated surface markers can be used to sort hepatocytes from defined lobule zones with high spatial resolution. We apply transcriptomics, miRNA array measurements and mass spectrometry proteomics to reconstruct spatial atlases of multiple zonated features. We demonstrate that protein zonation largely overlaps with mRNA zonation, with the periportal HNF4α as an exception. We identify zonation of miRNAs such as miR-122, and inverse zonation of miRNAs and their hepatocyte target genes, highlighting potential regulation of protein levels through zonated mRNA degradation. Among the targets we find the pericentral Wnt receptors Fzd7 and Fzd8 and the periportal Wnt inhibitors Tcf7l1 and Ctnnbip1. Our approach facilitates reconstructing spatial atlases of multiple cellular features in the liver and other structured tissues.

Introduction

The mammalian liver is a structured organ, consisting of repeating hexagonally shaped units termed ‘lobules’ (Fig. 1a). In mice, each lobule consists of around 9-12 concentric layers of hepatocytes[1]. Blood flowing from portal nodes (PN) at the corner of the lobules towards draining central veins (CV) generates gradients of oxygen, nutrients and hormones along the lobule radial axis. Additionally, Wnt morphogens are secreted by endothelial cells

---

[*]**Corresponding Author**: Correspondence to Shalev Itzkovitz, shalev.itzkovitz@weizmann.ac.il.
[2]Current affiliation: Institute of Molecular Cancer Research, University of Zurich, Zurich, Switzerland

Author Contributions
K.B.H. and S.I. conceived the study, S.B.M. and S.I designed experiments, S.B.M. prepared all the samples, S.B.M and Y.S. analyzed the data, A.E.M contributed to data analysis, R.M and T.V assisted with IF experiments, K.B.H contributed to establishing the method, S.I. supervised the study, S.B.M, Y.S. and S.I. wrote the manuscript. All authors reviewed the manuscript and provided input.

Competing Financial Interest
The authors declare no competing interest.

surrounding the CV, resulting in a graded morphogenetic field[2]. This graded microenvironment gives rise to spatial heterogeneity in gene expression among hepatocytes residing at different lobule layers, a phenomenon that has been termed ‘liver zonation’[3,4].

We have recently used spatially-resolved single-cell transcriptomics to uncover the global zonation patterns of hepatocyte gene expression[5]. We found that around half of all genes expressed in hepatocytes are zonated, with specific functional specialization that seem to match the zonated microenvironment. This global zonation suggests that similar spatial heterogeneity of hepatocytes may also exist for other cellular features, including proteins, metabolites and regulatory molecules such as microRNAs. However, achieving similar global zonation maps for cellular features beyond mRNA has encountered technical difficulties.

Immunohistochemistry enables measurements of protein levels with high spatial resolution but it is low-throughput and often limited by lack of availability of antibodies. Laser capture microdissection (LCM) and digitonin perfusion enable extracting large numbers of periportally or pericentrally enriched cells[6,7]. However, these techniques are limited in spatial resolution and purity, since they measure both hepatocytes and non-parenchymal cells. Single cell measurements of cellular features beyond mRNA are starting to emerge[8,9], however these technologies are less mature in tissues, compared to bulk RNA analysis. A methodology that would enable massive isolation of pure cell types from defined layers with high spatial resolution would enable generating organ-wide spatial atlases of key features such as methylation patterns, chromatin conformations, miRNA content and proteomics. In the liver, such measurements would broaden our understanding of the regulation of liver zonation and could be used to more precisely model liver metabolic function.

In this work, we developed an approach termed ‘spatial sorting’, that utilizes surface markers with discordant zonation profiles to isolate massive amounts of hepatocytes from defined lobule layers (Fig. 1b). We used these for high-throughput profiling of mRNAs, microRNAs and proteins (Fig. 1c), revealing novel features of liver zonation. These include a comprehensive proteomic zonation map and the identification of zonated miRNA with discordantly zonated target genes. Our approach can be readily applied to profile other cellular features of hepatocytes and other cell types in health and disease.

Results

Spatial sorting enables isolating bulk hepatocyte populations from different lobule layers

We used our recently reconstructed mRNA zonation map[5] to identify zonated surface markers with a large dynamic range in expression, spanning several radial lobule layers (Fig. 1a, Supplementary Fig. 1a). We argued that the combined staining of two inversely zonated surface proteins would be informative for inferring the lobule positions of single hepatocytes (Fig. 1b), which would facilitate cell sorting of many cells according to their spatial origin (Fig. 1b-c). CD73, encoded by the gene Nt5e, is an enzyme converting mononucleotides to nucleosides that exhibits pericentral zonation[5]. E-cadherin, a cell-cell adhesion glycoprotein encoded by Cdh1, exhibits periportal zonation[10] (Fig. 2a). We used immunofluorescence to validate the zonation of these two surface markers at the protein level as well (Fig. 2b-c).

We perfused livers of five ad-libitum-fed mice to dissociate single cells and performed fluorescence-activated cell sorting (FACS) of isolated hepatocytes stained with antibodies against CD73 labeled with APC and E-cadherin labeled with PE. We filtered hepatocytes by size and selected cells that were negative for the endothelial cell marker CD31 and the immune cell marker CD45, to avoid pairs of hepatocytes and non-parenchymal cells (NPCs)[11]. We further filtered out non-viable cells and selected tetraploid hepatocytes using Hoechst staining (Fig. 3a, Supplementary Fig. 1b). Stratifying hepatocytes by ploidy was important to obtain precise lobule localization (Supplementary Fig. 1c-d). The selected hepatocytes displayed strong anti-correlation in the fluorescence of CD73 and E-cadherin, as expected from the zonated expression patterns (Fig. 3b).

We defined eight gates based on the combined fluorescence of CD73 and E-cadherin (Fig. 3b). To ensure reproducibility, the gates were defined as percentiles of the marginal expression levels of each surface marker, compared to unstained control. To validate that our defined gates represent sequential lobule layers, we performed bulk RNA sequencing (RNAseq) on 10,000 sorted hepatocytes from each gate. Contamination of NPC RNA was negligible and uniform across all eight isolated populations, validating our isolation and sorting approach (Supplementary Table 1). We compared the zonation profiles obtained via spatial sorting to our spatially-resolved scRNAseq map[5]. Zonation profiles were highly concordant (Fig. 3c, Supplementary Table 2), demonstrating the feasibility of our approach for isolating bulk hepatocytes with high spatial resolution.

Mass spectrometry proteomic measurements of spatially-sorted hepatocytes

We next applied spatial sorting to reconstruct the zonation patterns of the hepatocyte proteome. To this end, we sorted 100,000 hepatocytes from each of the eight FACS gates and performed mass spectrometry proteomics. For each mouse and gate we also isolated 10,000 cells and applied bulk RNAseq. The Mass spectrometry measurements yielded 3,210 identified proteins (Supplementary Table 3). The hepatocyte protein content averaged over all FACS gates was highly correlated with previous bulk measurements[12] (Spearman's r = 0.75, Supplementary Fig. 2a). Our dataset included 3,051 proteins with matched mRNA (Supplementary Table 4). The means over all gates of the protein and mRNA levels were positively correlated (Spearman's r = 0.5, p-val = $1.2\text{x}10^{-181}$ n=3,051). Yet, for some proteins, there was a marked difference in protein and mRNA relative abundances (Fig. 4). These predominantly included hepatocyte secreted proteins. For example, Alb, encoding the secreted carrier protein albumin, was the most highly abundant hepatocyte mRNA (0.050±0.004 of cellular transcripts) but was ranked only 64 in protein levels (0.0034±0.0002 of cellular proteins). Other secreted proteins, which were ranked significantly higher in mRNA compared to the protein level included apolipoproteins encoded by Apoa1, Apoa2, Apoe, alpha-antitrypsin encoded by Serpin genes, complement system proteins and vitronectin, encoded by Vtn (Fig. 4a). A similar discordance between the levels of mRNAs and proteins for secreted genes was previously observed in mammalian cell lines [16]. Ribosomal mRNAs and proteins had a protein to mRNA ratio close to one, whereas genes of the TCA cycle had substantially higher protein to mRNA levels (Fig. 4b, Supplementary Fig. 2). Cps1, encoding the urea cycle enzyme carbamoyl-phosphate synthase was ranked first in protein content (0.0682±0.0066), but only 478 in mRNA expression ($2.88 \times 10^{-4} \pm 5.4 \times 10^{-5}$ of cellular transcripts, Fig. 4a). Thus, the relative expression levels of mRNAs and proteins differ for distinct functional classes.

Zonation patterns of the hepatocyte proteome

We next examined whether the hepatocyte proteome exhibited zonated patterns. We found that 55% of the hepatocyte proteins (1,672 out of 3,051) were significantly zonated ($FDR<0.05$, Kruskal-Wallis test, Fig. 5a). Periportal and pericentral enriched KEGG pathways largely recapitulated previous zonation studies. Bile acid biosynthesis, lipid metabolism and P450 xenobiotic metabolism were pericentrally zonated, while gluconeogenesis, oxidative phosphorylation and complement and coagulation cascades were periportally zonated (Supplementary Fig. 3). We validated the measured protein zonation using immunfluorescense for representative pericentral and periportal proteins (Supplementary Fig. 4).

The combined measurements of both mRNA and proteins from the same spatially-sorted gates enabled a controlled comparison of protein and mRNA zonation patterns (Fig. 5b-c). The periportal biases (the difference between the expression in the periportal and pericentral gates divided by the mean expression) were significantly correlated between mRNA and proteins, indicating similar mRNA and protein zonation profiles for most genes (Spearman's $r = 0.39$, p-val = 1.45×10^{-110} for all proteins, $r=0.45$, p-val = 1.71×10^{-79} for highly expressed proteins, Fig. 5b-c). Notably, some genes exhibited discordant zonation of mRNAs and proteins. These included genes that were zonated at the protein but not mRNA level, such as Rbp4, Idh3b, Mrpl43 and genes that were zonated at the mRNA but not at the protein level, such as A1cf, Clmn and Lsr (Fig. 5c). The discordant genes also included Hnf4a, a key hepatocyte transcription factor[4,17]. The mRNA levels of Hnf4a were not zonated, whereas the protein content was higher in the periportal gates (Supplementary Fig 4c). This periportal protein bias is in line with previously reported involvement of Hnf4a in periportal repression of Wnt regulated pericentral genes[17–19] and induction of periportally expressed targets[20]. Indeed, we found that in Hnf4a KO mice[21], periportal genes were preferentially downregulated compared to WT controls, whereas pericentral genes did not have preferential differential regulation (Fisher exact test p-val = 1.16×10^{-4}, Supplementary Table 5). Thus, our analysis indicates that the majority of proteins and mRNAs are similarly zonated, and highlight genes with potential post-transcriptional regulation.

Zonation of the hepatocyte miRNA content

We next asked whether spatial sorting could be used to explore the regulatory mechanisms that shape hepatocyte zonation. miRNAs are short RNA oligonucleotides, roughly 22 bp long, that target specific mRNAs through Watson-Crick base-pairing, leading to increased degradation or decreased translation of target transcripts[22]. Regulation by miRNAs seems to be important in liver development, metabolism and homeostasis[23,24]. Notably, miRNA regulation may impact liver zonation, as mice lacking the miRNA central processing element Dicer in hepatocytes exhibit profound changes in zonation patterns[25]. We reasoned that combined global measurements of the zonation profiles of miRNAs and mRNAs could identify potential miRNA-target regulatory interactions through the detection of miRNA-target pairs with anti-correlated expression profiles[26].

To this end, we performed miRNA microarray measurements of spatially sorted hepatocytes from three mice. We detected 302 miRNAs that were expressed in hepatocytes in all three mice. We further focused on 137 miRNAs that were classified as “high confidence” in miRBase[27]. 45% (61/137) of these high-confidence hepatocyte-expressed miRNAs were significantly zonated (FDR ≤ 0.2, Kruskal-Wallis test with Benjamini-Hochberg correction, Fig. 6a). Most zonation profiles (48/61) were mildly pericentral with a center of mass (COM) between 4-4.5, while seven others showed strong periportal zonation (COM ≥ 6). We measured the expression of six of the miRNAs predicted to be zonated using qRT-PCR, obtaining excellent correspondence with the microarray measurements (mean Spearmans’ r = 0.70±0.24, Fisher’s method $p = 1.0 \cdot 10^{-15}$, Fig. 6b).

The zonated miRNAs included miRNAs previously described to play a role in liver development, metabolism and regeneration. MiR-122-5p, the most abundant miRNA in our measurements, in agreement with previous studies[28], comprised 46.5±3.5% of the total miRNA content in hepatocytes. We found that miR-122-5p was periportally zonated, with a 1.15-fold higher expression in the periportal gates compared to the pericentral gates (p-value < 0.01, Kruskal-Wallis test, Supplementary Table 6). We confirmed the zonation of miR-122-5p with qRT-PCR (Spearman’s r = 0.79, Figure 6b). miR-122-5p was significantly anti-correlated with its targets compared to randomized genes (Supplementary Fig. 5), indicating a potential regulatory role in shaping their zonation. Prominent pericentral miR-122-5p targets (genes that were repressed in their expression in the periportal layers in which miR-122 was more abundant) included the canonical miR-122-5p target gene Cs, encoding citrate synthase, as well as Klf6 and Slc35a4 [29] (Supplementary Fig. 5). MiR-30a-5p exhibited periportal zonation (periportal to pericentral ratio of 1.19, Kruskal-Wallis p=0.007, Fig. 6a, Supplementary Table 6). Mtdh, a known target of miR-30a-5p, previously shown to change in expression in liver tumors [30], was pericentral, inversely zonated to its miRNA regulator (Spearman’s r = -0.81, p = 0.022, Supplementary Table 7). Additional zonated miRNAs included the pericentral miR-103-3p and miR-107-3p and the periportal miR-802-5p, which have been previously shown to modulate hepatic glucose sensitivity [31,32] (Fig. 6a). In summary, our measurements revealed profound zonation of key hepatic miRNAs.

Detection of putative miRNA-regulated hepatocyte target genes using zonation profiles

Spatially-stratified measurements of miRNAs and mRNAs could be used to identify potential miRNA regulation at the mRNA degradation level. Such regulation would be manifested in inverse correlations between the zonation profiles of a target mRNA and its regulating miR(s). To identify such interactions, we constructed a miRNA-mRNA regulatory network based on predictions from TargetScan[33] (Supplementary Table 7). We included all highly-expressed hepatocyte genes and interactions with high confidence, and filtered out genes that are not predicted to be regulated by highly-abundant miRNAs. The resulting network included 3,502 interactions between 131 miRNAs and 588 genes. For each gene, we constructed the cumulative regulating miRNA profile, by summing up the zonation profiles of all miRNAs with a predicted regulatory interaction for the considered target gene (Supplementary Table 8). We computed the Spearman correlation between the gene’s mRNA zonation profile and the cumulative miRNA zonation profile and compared it to randomized degree-preserving networks (Fig. 7a).

Our analysis identified 11 genes that were significantly more anti-correlated with their regulating miRNAs compared to random ($FDR \leq 0.2$, Supplementary Table 8, Supplementary Fig. 6). Pericentral target genes included Acat1, which encodes the mitochondrial enzyme acetyl-CoA acetyltransferase 1, an important enzyme in ketone and isoleucine metabolism. Periportal target genes included Alpha-1-acid glycoprotein 1 (AGP1), and Alpha-1-acid glycoprotein 2 (AGP2), encoded by the genes Orm1 and Orm2 respectively, which are secreted plasma carrier proteins that were significantly anti-correlated with all of their regulating miRNAs - miR-20a-5p, miR-20b-5p, miR-93-5p and miR-106b-5p (mean Spearman's $r = -0.994 \pm 0.011$, Fisher's method $p < 10^{-14}$, Fig. 7b). Another significantly anti-correlated periportal gene was Ly6e, encoding the protein lymphocyte antigen 6E (Supplementary Fig. 6).

Regulation of Wnt signaling components by miRNA

Wnt is a major factor that shapes hepatocyte zonation[34–39]. Wnt and Rspondin morphogens are secreted by pericentral liver endothelial cells[2,11,40–42], resulting in higher pericentral expression of Wnt-activated genes and lower pericentral expression of Wnt-inhibited genes [5,34]. Notably, hepatocyte-specific Dicer knock-out mice have perturbed zonation of Wnt-regulated genes, such as Glul and Arg1[25]. This suggests that miRNAs could differentially modulate hepatocyte Wnt signaling in different lobule zones. To explore this hypothesis we analyzed the miRNA-target sub-network that includes genes associated with Wnt signal processing (Methods, Fig. 7c-d). This analysis uncovered several key components of the Wnt network that exhibit zonation in hepatocytes and that have spatially-anticorrelated zonated miRNAs. The Wnt receptors Fzd7 and Fzd8 were more highly expressed in pericentral hepatocytes, whereas their regulating miRNAs miR149-5p, miR-30a-5p, miR-30a-3p, miR-21a-5p, miR-99a-5p and miR-100-5p were more abundant in periportal hepatocytes. In contrast, inhibitory components of Wnt signaling such as Ctnnbip1 and Tcf7l1 were periportally zonated. Tcf7l1, also known as Tcf3, is a transcriptional repressor of Wnt-activated genes that is inactivated by binding of β-catenin[43]. This periportally zonated gene is anti-correlated with its regulators miR-212-3p, miR-423-5p and miR-5107-5p (Fig. 7d). Ctnnbip1, encoding β-catenin interacting protein, prevents the binding of β-catenin to TCF7L1 and thus its removal and activation of Wnt target genes[44]. The miR regulators of this periportal gene, miR-188-5p and miR-3102-5p, were pericentrally-zonated (Fig. 7d). Our analysis thus highlights zonated components of hepatocyte Wnt signaling and their potential regulation by miRNAs.

MicroRNA zonation and diseased liver states

Many liver pathologies exhibit zonated damage, born out of the differential susceptibilities of periportal and pericentral hepatocytes to different insults[45]. MiRNA are attractive biomarkers, due to their relative stability and high concentrations in the circulation. Therefore, we sought to explore whether the blood levels of zonated miRNA could be indicative of such zonated damage. Acetaminophen (APAP) intoxication leads to necrosis of pericentral hepatocytes. We analyzed published miRNA levels measured in bulk liver and plasma of APAP-treated mice[46] and found that almost all pericentral miRNAs were enriched in plasma, and depleted in liver of APAP-treated mice relative to controls ($p = 0.05$, Wilcoxon test, Supplementary Fig. 7), whereas periportal miRNAs were not significantly enriched or depleted in plasma vs. liver samples ($p = 0.43$, Wilcoxon test, Supplementary Fig. 7).

Hepatocellular carcinoma (HCC) is often associated with activation of the Wnt pathway in hepatocytes[38,47]. Wnt activity is pericentrally-zonated in the healthy liver. Our study revealed zonated Wnt components such as the pericentrally-zonated Wnt receptors Fzd7 and Fzd8 and the periportally-zonated Wnt inhibitors Ctnnbip1 and Tcf7l1. We found that these components are potentially modulated by zonated miRNA, thus we hypothesized that perturbations in these miRNAs might be implicated in the carcinogenic process. To this end, we analyzed the hepatocellular carcinoma (LIHC) dataset of The Cancer Genome Atlas[48]. We found that periportally zonated miRNAs were down-regulated whereas pericentrally zonated miRNA were up-regulated (correlation of Spearman's $r= -0.29$ between the miRNA zonation profile center of mass and the log-fold change between tumors and normal tissue, $p = 0.0061$, Supplementary Fig. 8). For example, miR-99a and miR-100 which potentially inhibit Fzd8 expression in the periportal zones, were down-regulated in tumors (log2 fold change = -1.34 and -0.63, respectively, Kruskal-Wallis $p = 2.2 \cdot 10^{-16}$ and $p = 2.6 \cdot 10^{-4}$, respectively). Conversely, miR-93, that potentially inhibits the Wnt inhibitor Tcf7l1 in the pericentral zone, was up-regulated (log2 fold change = 1.49, $p = 5.4 \cdot 10^{-20}$) (Supplementary Fig. 8). The anti-correlation between miRNA fold change in HCC and its zonation in the normal liver became even stronger when focusing on patients without Wnt activating somatic mutations (Spearman's $r = -0.36$, $p = 4.5 \cdot 10^{-4}$, Methods). Such increased inverse correlation could indicate that miRNA may play a role in activating the Wnt pathway independently of somatic mutations in the Wnt pathway.

Discussion

The liver exhibits profound division of labor among hepatocytes that reside at different zones. Understanding and modeling liver function thus requires characterization of hepatocyte functions at each lobule coordinate. In this study, we present spatial sorting, a generic approach to isolate large amounts of hepatocytes with high spatial resolution for a broad range of downstream measurement modalities. The approach utilizes zonated surface markers that can be identified by spatially resolved transcriptomic atlases. We demonstrated applications of this approach for resolving the zonation of hepatocyte proteins and miRNAs. The approach can be readily applied to other structured organs and cells types exhibiting zonation, including liver endothelial cells[11], intestinal enterocytes[49] and kidney cells[50,51]. The usage of endogenous surface markers renders spatial sorting particularly useful for studying zonation in humans as well.

Our proteome analysis revealed some notable discordance between the average hepatocyte levels of proteins and mRNAs, mostly for genes encoding secreted proteins (Fig. 4). In contrast, we found that the protein zonation profiles highly overlap those of the mRNAs. These results argue for a predominance of spatial regulation of hepatocyte protein levels via transcription or mRNA stability, rather than through translational control or protein stability.

Hnf4a, a key hepatic transcription factor, was among the small group of genes for which protein and mRNA zonation profiles were discordant. Hnf4a mRNA was expressed in a non-zonated manner, whereas its protein levels were periportally zonated. This fits with previous reports of periportal expression of Hnf4a hepatocyte target genes[4,18–20]. Notably, Hnf4a is a transcriptional activator of miR-122[52], the most abundant liver-expressed miR, which we also found to be periportally zonated. Due to sensitivity limitations of mass spectrometry proteomics our proteomic measurements did not include low-abundance genes, including other key liver transcription factors, which may exhibit higher levels of post-transcriptional regulation.

Recent works have begun to develop in-silico multi-scale models for predicting the liver's response to stimulations by metabolites and xenobiotics[53–55]. These models consider multiple units representing hepatocytes at different zones that exchange materials and process them through individualized metabolic networks, thus modeling the polarized blood perfusion throughout the lobule. Future incorporation of the zonated levels of enzymes into such models could increase their precision and better capture in-vivo fluxes. Our proteomic map provides such detailed zonation of key enzymes (Supplementary Table 3).

Our work provided a global spatial atlas of miRNA zonation, identifying key hepatocyte zonated miRNAs such as miR-122-5p and miR-30a-5p. We used the combined miRNA and target mRNA levels to identify potential regulatory interactions that could entail zonated mRNA degradation. This forms an important resource that should be validated in future studies. miRNAs have been shown to be highly dynamic along the course of several diseases such as fibrosis, viral infection and liver cancer [24,56,57]. Spatial sorting could be used to measure the zonation of these miRNAs along the courses of these diseases. Moreover, our analyses of APAP-treated mice show that plasma measurements of zonated miRNAs could potentially be used as biomarkers to identify zonated liver damage[58,59].

Wnt is a key regulator of hepatocyte zonation[2,34,38]. The pericentral secretion of Wnt morphogens by endothelial cells generates a zonated external morphogen field, which could explain a significant fraction of the zonated hepatocyte genes. Our study revealed that in addition to the Wnt signal, the hepatocyte Wnt sensing and processing machinery also seems to be zonated. We identified pericentral zonation of the key Wnt receptors Fzd7 and Fzd8 and periportal zonation of the Wnt inhibitors Tcf7l1 and Ctnnbip1. This joins previous reports of periportal zonation of APC, a key Wnt regulator[34]. Our study further identified miRNAs that regulate these zonated Wnt components. Thus miRNAs seem to be upstream of Wnt signaling. These results could explain the effects of hepatocyte-specific Dicer KO and beta-catenin KO. While Dicer KO resulted in perturbed zonation of Wnt targets, beta-catenin KO did not substantially alter miRNA levels[25]. Our finding of decreased expression of miRNA that may potentially inhibit Wnt receptors (miR-99a and miR-100) in HCC could indicate that Wnt-targeting miRNA may play a role in the liver carcinogenic process.

Our approach enables attaining up to a few hundreds of thousands of hepatocytes per sorted population. While this amount is compatible with a broad range of assays, it is insufficient for assays that require massively larger amounts of material, such as RNA methylations[60] and metabolic profiling[61]. Moreover, since the approach is FACS-based, measuring metabolites, which are labile, would be compromised by the substantial incubation periods involved in the protocol[62]. Nevertheless, it will be interesting to apply spatial sorting to explore additional zonated hepatocyte features, including chromatin modifications, DNA methylations, three-dimensional chromosomal conformations, DNA mutation spectra and chromosomal aberration. Such measurements could resolve hepatocyte cell identity, regulatory mechanisms and susceptibility to damage in each zone.

Methods

Animal experiments

Mouse experiments were approved by the Institutional Animal Care and Use Committee of the Weizmann Institute of Science and performed in accordance with institutional guidelines. Sorting experiments were conducted on five three-months-old C57BL/6JOlaHsd male mice, obtained from Envigo (Israel). Mice were fed ad libitum and were kept in a reverse light-dark cycle. Mice were anaesthetized with Ketamine (100 mg kg−1) and Xylazine (10 mg kg−1) dissolved in 1xPBS and injected intraperitoneally 6h-9h after lights off (ZT 18-21).

For imaging experiments, livers of three-months-old C57BL/6J male mice, obtained from Envigo (Israel), were harvested and fixed in cold PFA for 3h at 4°C followed by overnight fixation in cold PFA + 30% sucrose at 4°C while revolving. Livers were embedded in OCT (Tissue-Tek) the next morning. Blocks were kept at -80°C.

Immuno-Fluorescence of CD73 and E-cadherin

OCT embedded mouse liver blocks were sectioned into 7um thick slices. Slices were fixed with cold Methanol for 20min. After three 5min washes with PBST (1X PBS, 1% BSA + 0.1% Tween), sections were permeabilized by 10min incubation at room temperature with PBSTX solution (1X PBS, 0.25% Triton 100X and 1% BSA). Slices were then washed again as before and were incubated for 1h at room temperature with blocking solution (1x PBS, 0.1% Tween and 5% Goat/Normal Horse Serum). Slices were next incubated with the antibody solution (blocking solution with 1:50 antibody in a total reaction volume of 150ul) at 4 °C overnight. Antibodies used were Alexa Fluor 647 rat anti-mouse CD73 (BD, cat: 561543) and Alexa Fluor 555 mouse anti-Ecadherin (BD, cat: 560064). On the next day, slices were washed with PBST 3 times. Nuclei were stained with DAPI (1:100 in PBS, 10mis). Imaging of liver porto-central axis was performed on a Nikon-Ti-E inverted fluorescence microscope with a 100× oil-immersion objective and a Photometrics Pixis 1024 CCD camera using MetaMorph software using the scan stage option.

Z-projected images of lobule scans (8 scans, 3 mice) were analyzed. Membrane segments of hepatocytes were measured for the intensity of Alexa Fluor 555 (E-cadherin) and Alexa Fluor 647 (CD73). Background, set as the paired cytoplasmic intensity for each membrane signal was subtracted. Segments were then binned into eight groups representing eight lobule layers (1 = pericentral, 8 = periportal), according to their radial distance from the central vein. Median intensity of the segments from each lobule layer was calculated and averaged over the different lobules (Fig. 2b-c). Values were scaled from 0 to 1 and the plot was smoothened with a sliding window of 3.

Immuno-Fluorescence of Aldob and GS

Immuno-fluorescence of Aldolase b (Thermo-Fisher, cat: PA5-30218) and Glutamine Synthetase (Thermo-Fisher, cat: MA5-27749) was perform in similar method to E-cadherin and CD73, however to these primary antibodies, secondary antibodies were needed – after overnight incubation with the primary antibodies, slides were incubated 2h at room temperature with secondary antibodies prior to dapi stain. For Aldob antibody we used 1:500 Goat anti-Rabbit IgG (H+L) Cross-Adsorbed Secondary Antibody conjugated to Cy3 (Thermo-Fisher, cat: A10520). For GS antibody we used 1:500 Goat anti-Mouse IgG (H+L) Cross-Adsorbed Secondary Antibody conjugated to Cy3 (Thermo-Fisher, cat: A10521).

Immuno-Fluorescence of Hnf4α

Hnf4a antibody staining was done according to a previously published protocol[63]. Paraffin embedded liver blocks were sectioned into 10um-thick sliced. Slides were deparaffinised and rehydrated, followed by a methanol incubation for 5 minutes. Slides were then incubated in in citrate buffer (pH 5.8-6.0) for 30 minutes at 100°C for heat-induced epitope retrieval. Blocking of non-specific binfing sites was done by 1h incubation with PBS, 10% BSA and 0.3% triton, after which slides were incubated overnight with HNf4a antibody (R&D, cat: PP-H1415-00) in a dilution of 1:350 in blocking solution at 4°C. Slides were incubated for 2h in 1:700 Donkey anti-Mouse IgG (H+L) Highly Cross-Adsorbed Secondary Antibody, conjugated to Alexa Fluor 594 (Thermo-Fisher, cat: A-21203) with 1:1000 DAPI.

Liver Perfusions and hepatocytes dissociation

Once anaesthetized, mice livers were perfused as previously described[64], with a few adjustments. A 27G syringe, connected to the perfusion line and pump, was inserted into the vena cava. 25ml of pre-warmed to 37°C EGTA buffer followed by 25ml of pre-warmed to 37°C EBS buffer with 2.3U of Liberase Blendzyme 3 recombinant collagenase (Roche Diagnostics) were cannulated into the vena cava. Shortly after the beginning of the perfusion, the portal vein was cut to allow drainage of the blood.

After perfusion of 10ml of EGTA and 15ml of the enzyme solution, livers were explanted into a Petri dish with 25ml of pre-warmed EBS and gently minced using forceps. Dissociated liver cells were collected and filtered through a 100um cell strainer. Cells were spun down at 30rcf for 3 min at 4°C to get hepatocytes enriched pellet. Pellet was resuspended in 25ul cold EBS.

Cell Staining

To discard dead hepatocytes, 22.5ml Percoll (Sigma) mixed with 2.5ml 10x PBS was added to the cells. Cells were centrifuged at 600rpm for 10 minutes. Supernatant containing the dead cells was aspirated and cells were resuspended in pre-warmed Hoechst buffer (DMEM + 10% FBS + 10mM Hepes). After counting, concentration was adjusted to $2x10^6$ cells in 1ml. To determine ploidy of hepatocytes, DNA was stained with Hoeschst (15ug/ml). Resperine (5uM) was also supplemented to the cells to prevent Hoechst expulsion from the cells. Cells were incubated 30min at 37°C. Hepatocytes were centrifuged for 5min in 1000rpm at 4°C and supernatant was discarded. Next, cells were stained with Alexa fluor 488 Zombie green (BioLegend) to later enable the detection of viable cells by FACS. Cells were resuspended in cold PBS in a concentration of 10^6 cells in 100ul. Zombie-green was added in a dilution of 1:500. Cells were kept in a rotator in the dark at room temperature for 15min. After spinning down (1000rpm, 5min, 4°C), cells were resuspended in FACS buffer (2mM EDTA pH 8 and 0.5% BSA in 1xPBS), in a concentration of 10^6 cells in 100ul. Cells were stained with PE-anti-E-cadherin (BioLegend, cat: 147304), APC-anti-CD73 (BioLegend, cat: 127210), PE-Cy7-anti-CD31 (BioLegend, cat: 102418) and APC-Cy7-anti-CD45 (BioLegend, cat: 103116), in a dilution of 1:300. FcX blocking solution (BioLegend) was added in a dilution of 1:50.

Flow Cytometry and sorting

Cells were sorted by SORP-FACSAriaII sorter (BD) using a 130 μm nozzle and 1.5 natural density (ND) filter. Lasers compensation was corrected manually. In order to collect eight populations, each enriched with spatially-stratified hepatocytes with equal viability and ploidy levels, events were screened through the following five nested gates (Fig. 3a-b, Supplementary Fig. 1b-d): (1) hepatocytes gate from all events – set by plotting FSC-A against SSC-A and excluding large clusters and small debris; (2) singlets FSC – set by excluding the margins of FSC-A and FSC-W plot; (3) singlets SSC – excluding upper margins of SSC-W when plotted against SSC-A; (4) live cells gates according to the Zombie-488 negative cells, comparable to unstained cells; (5) hepatocytes only, by depleting CD31 and CD45 (markers of NPCs), and (6) tetraploid hepatocytes, inferred by Hoechst histogram (Fig. 3a-b, Supplementary Fig. 1c-d). Hepatocyte size and overall protein content scale with ploidy[65], thus creating spurious correlations between the zonated surface markers (Supplementary Fig. 1c-d). Sorting without ploidy stratification would result in inclusion of hepatocytes from different lobule layers, reducing spatial accuracy (Supplementary Fig. 1c-d).

We then plotted PE-intensity for E-cadherin staining and APC-intensity for CD73 staining. The positively stained cells were determined by measuring the intensities for unstained cells. The highest intensity for unstained cells was the threshold for the positively stained cells. Each population, CD73 positive and E-cadherin positive, was further gated to four equal subpopulations, representing graded intensities of the marker. Thus, subpopulations 1, 2, 3 and 4 had equal amount of events, 1 had the highest APC-CD73 intensity while 2, 3, 4 had gradually decreasing intensities of APC. Likewise, subpopulations 5, 6, 7 and 8 were equally distributed, 8 having the highest PE-E-cadherin intensity while 7,6,5 had gradually decreasing PE intensities. Populations 4 and 5 contained cells from below positive intensity threshold, to accurately resemble mid lobule hepatocytes, in which both CD73 and E-cadherin abundances are very low (Fig. 2). All gates were set for each of the five experiments independently, with a large overlap.

10,000 hepatocytes from each gate were sorted into Dynabeads mRNA DIRECT Micro Kit lysis buffer (Invitrogen) for RNA sequencing. After sorting, cells were spun down and frozen at -80°C until processing. 100,000 hepatocytes from each population were collected into FACS buffer, and resuspended twice with PBS to wash away serum proteins. Pellets were flash frozen and sent to Mass spectrometry proteomics measurements (The Smoler Protein Research Center, Technion, Israel). Additional 50,000 cells were collected for miRNA microarray. Total RNA was isolated using Direct-zol RNA microprep kit (Zymo Research).

RNA sequencing

10,000 hepatocytes from each sorted population were collected for library preparation. Cells were sorted into Lysis buffer supplied in Dynabeads mRNA Purification Kit (Invitrogen, cat: 61006). RNA was extracted by the kit according to the provided protocol. 2ul of the extracted mRNA from each sample were used for libraries. Library preparation was done with mcSCRBseq protocol[66]. The cDNA was pre-amplified with 10-15 cycles, depending on cDNA concentration indicated by qPCR quality control. 2ng of the amplified cDNA was converted into sequencing library with the Nextera XT DNA Library kit (Illumina, FC-131-1024), according to supplied protocol. Quality control of the resulting libraries was performed with an Agilent High Sensitivity D1000 ScreenTape System (Agilent, 5067-5584). Libraries were loaded with a concentration of 2.2pM on 75 cycle high output flow cells (Illumina, FC-404-2005) and sequenced on a NextSeq 500 (Illumina) with the following cycle distribution: 8bp index1, 16 bp read1, 66 bp read2 (no index2 needed). Total 40 libraries, eight sorted populations for five different mice were sequenced.

Sequencing analysis pipeline

Illumina output files were demultiplexed with bcl2fastq 2.17 and the resulting fastq files of mRNA sequencing experiments were analyzed with the zUMIs pipeline[67]. Reads were aligned using STAR to a transcriptome index of the GRCm38 release 84 (Ensembl) and exonic UMI counts per million (CPM) were calculated with pipeline default settings and TMM normalization[68] implemented in EdgeR[69]. 14,027 transcripts were identified in the experiment over the 40 libraries. Data were further normalized by dividing each sample by its sum of CPM. Two out of the 40 libraries failed to reach over 200K reads and were discarded (m2_2_cpm and m3_5_cpm samples in Supplementary Table 2).

Mass spectrometry

Fourty samples (five mice, eight populations each) were digested by trypsin and analyzed with LC-MS/MS on Q Exactive plus (Thermo). The data were analyzed with MaxQuant 1.5.2.8[70] against the mouse Uniprot database. Data were quantified using the same software. We retained proteins with FDR <0.01 in at least 2 samples in one of the eight groups, identified by at least 2 peptides across all samples. 3,210 proteins were identified. For each sample, LFQ intensities for each peptide were normalized by the sum of all intensities – yielding expression fraction out of the total protein detected.

Analysis of potential non-parenchymal cells (NPC) representation

Although we used negative selection with surface markers for endothelial cells (CD31) and immune cells (CD45), we computationally validated that there is no significant presence of NPCs in our sorted populations. To this end, we compiled a gene expression dataset of nine major liver cell types from previous publications[11,71], including endothelial cells, T cells, plasmacytoid dendritic cells (pDCs), Kupffer cells, liver capsule macrophages (LCM), B cells, neutrophils, hepatocytes[11] and cholangiocytes[71].We filetered the dataset to include only genes with transcriptome fraction of at least 10^{-5} in at least one cell type, and which are present in our spatially-sorted hepatocyte RNA-Seq data, resulting in 9,805 expressed genes. We next identified the top 100 marker genes for each of the nine cell types, defined as having the largest ratio between their expression in a given cell type and the maximum expression over all other cell types (Supplementary Table 1). The summed expression of the marker genes, which we termed the cell types' "signature", was calculated for both the transcriptomic and proteomic data of our sorted populations. In the transcriptomic data, the hepatocyte signature made up 15.7±1% of the spatially sorted populations, while each of the other cell types' signatures comprised only 0.075-0.27% of the transcriptomic signature matrix in each FACS gate, indicating a 100-fold ratio between unique hepatocyte signature contribution and that of other cell types. Importantly, there were no significant differences in the levels of the cell type signatures across the spatially-sorted populations (Kruskal-Wallis $p = 0.99$). In the proteomic data, the hepatocyte signature made up 4.5±0.8% of the total protein content, while each of the other cell-types' signatures comprised only 0.0004-0.4113% of the protein content. Likewise, there were no significant differences in the levels of the proteomic cell type signatures across the spatially-sorted populations (Kruskal-Wallis $p = 1$).

Calculating zonation of Hnf4a targets

We used the data of Holloway at al.[21] for differentially expressed genes in male mice with Hnf4α KO compared to WT male mice. We extracted a unique list of these genes and calculated the Benjamini-Hochberg FDR to identify significantly differentially-expressed genes, set to be with $FDR < 0.01$. Those genes were intersected with our spatial sorting RNA-seq data, resulting in 1,166 genes. We next grouped the genes according to the following categories: genes were considered downregulated or upregulated if their KO/WT $\log_2$ fold change was smaller than -1 or greater than 1, respectively; genes were considered pericentral/periportal, according to our spatial sorting RNAseq data, if their zonation center of mass was smaller (PC) or larger (PP) than 4.5 respectively. These criteria formed 4 groups – upregulated pericental genes (296 genes), upregulated periportal genes (123 genes), downregulated pericental genes (348 genes) and downregulated periportal genes (245 genes). We used Fisher's exact test to identify a non-random association between differential expression and zonation under Hnf4a-KO ($p = 1.2\text{x}10^{-4}$).

miRNA microarrays

Total RNA (100ng), isolated from bulk populations of 50,000 spatially-sorted hepatocytes ($n = 3$) per FACS gate, was labeled with Cy3 during transformation into cDNA using an RNA Agilent miRNA Labeling Kit (Agilent, UK) and Spike Kit (Agilent, UK). cDNAs were hybridized to Mouse miRNA Microarray, Release 21.0, 8x60K (v21) microarray slides (Agilent, UK) according to Agilent microRNA Hybridization Kit protocol (Agilent, UK) and scanned using Agilent G2505B array scanner. Data were extracted using the Feature Extraction software (Agilent, UK) with default parameters.

qRT-PCR

Total RNA, isolated from bulk populations of 50,000 spatially-sorted hepatocytes ($n = 3$) per FACS gate, was diluted to 5 ng/μL, and cDNA was reverse-transcribed using the miRCURY LNA RT Kit (Qiagen, cat. no. 339340) according to the manufacturer's instructions on an Applied BioSystems ProFlex PCR System. Plates were prepared using the miRCURY SYBR Green PCR Kit (Qiagen, cat. no. 339346) with custom miRCURY LNA PCR primers (Qiagen cat. no. 339306, Supplementary Table 10). Each 10 μL reaction volume contained 5 μL 2x miRCURY SYBR Green Master Mix, 0.5 μL ROX reference dye, 1 μL PCR primer mix, 0.5 μL RNAse-free water and 3 μL of cDNA sample diluted 1:60. qPCR reactions and measurements were performed on a StepOne Real-Time PCR System (Thermo Fisher, cat. no. 4376357) according to the manufacturer's instructions. Correlations between qRT-PCR and microarray measurements were calculated on a mouse-by-mouse basis.

Center of mass calculation

The center of mass (COM) of an expression profile x (spread over $z = 1{:}8$ FACS gates) was calculated as:

$$COM(x) = \frac{\sum_{z=1}^{8} Z \cdot x_z}{\sum_{z=1}^{8} x_z} \qquad \text{(Equation 1)}$$

This formula yields a number $COM \in [1,8]$ that indicates around which gate most of the expression is distributed.

Comparing bulk mRNA with published scRNAseq

Spatial sorting produces sub-populations of hepatocytes that are enriched for specific lobule layers, however each FACS gate includes several lobule layers. To compare the bulk mRNA measurements of the FACS-gated sub-populations to the zonation measurements previously reconstructed using spatially-resolved single-cell transcriptomics[5] we thus computationally estimated the center of mass, namely the weighted average of all single cells represented by each gate. To this end, we implemented Cibersort (https://cibersort.stanford.edu/ [72], to estimate the relative abundances of each lobule layer in the sorted subpopulations. We extracted a gene signature list for each layer from the scRNA seq data [5]. A total of 17 genes with mean expression greater than 5×10^{-5}, zonation FDR smaller than 0.01 and dynamic range of at least 10-fold between the mean of the two periportal layers and the mean of the two pericentral layers was used for the analysis. The means of five mice of the zonation profiles of these genes across the eight sorted gates were used as the mixed-populations data set. The relative abundances of each of the nine layers in each of the eight sorted population was calculated (with 'Disable quantile normalization' option checked). Fig. 3c presents the mean expression in each FACS gate over five mice (blue) and mean expression in scRNA seq data[5], weighted by the relative abundances of each layer in each FACS gate (yellow).

Comparing proteins and RNA

Out of the 3,210 proteins (Supplementary Table 3) detected in Mass spectrometry and 14,027 mRNAs (Supplementary Table 2) detected in RNA-sequencing, 3,051 were found in both datasets (Supplementary Table 4). The median expression fraction of five mice was calculated for each gate in each measurement. We scatter-plotted the averages over all gates of the eight mRNA medians and eight protein medians for every gene and found a Spearman correlation r = 0.50 (0.48-0.50 per each gate independently). In order to better characterize mRNA and protein ratios in different KEGG pathways[73], we plotted the regression line of protein by mRNA. The residual of the proteins from the regression line was calculated and grouped according to KEGG pathways (Fig. 4b, Supplementary Fig. 2).

Computing zonation

For each of the 3,051 common proteins and mRNAs, Kruskal-Wallis test was performed to check for variability between different sorted gates (n= 40 populations, 5 mice in each of the 8 gates, df =37). To correct for multiple hypotheses, we performed the Benjamini–Hochberg procedure to obtain the FDR for each hypothesis. We classified proteins as zonated if they had FDR < 0.05. 1,672 were significantly zonated. To produce the protein zonation heatmap (Fig. 5a), we first removed all proteins which have a median of LFQ = 2^{18} in any of the eight gates (479 proteins). Next, we normalized all protein profiles to their maximum across all FACS gates and sorted them by their center of mass (Fig. 5a).

Microarray data

Only miRNAs that were annotated as “high confidence” in miRBase v22 (downloaded 30/10/18) were kept for analysis. The raw signal for each miRNA in each FACS gate and in each array was normalized by the total signal per gate per array. Only miRNAs present in all three biological replicates were retained for further analysis, and their initial normalized signal was averaged over all arrays. Finally, the averaged signal was divided again by the total signal in each gate (this operation amounted to dividing by a number very close to 1, since only miRNAs with very low expression were not present in only some of the replicates). MiRNA zonation was inferred using the Kruskal-Wallis test (for each miR, comparison of 8 gates, with each having 3 replicates, df=21), and applying a Benjamini-Hochberg correction on the p-values obtained from the KW test. MiRNAs with FDR ≤ 0.2 were classified as zonated.

Differential zonation of miR-122-5p targets

Targets of miR-122-5p were taken from Tsai et al. (2012)[29]. 146 of the targets listed were expressed in our liver zonated transcriptome data. The mean COM was calculated for these targets and for 1,000 random samplings (with replacement) of 146 liver-expressed genes (genes with maximal expression over all gates that was at least 4×10^{-6} of transcriptome). We performed a Wilcoxon rank-sum test for the COMs of the target genes vs. COMs of randomly sampled genes, yielding p = 0.018.

Analysis of acetaminophen-induced liver injury (APAP-DILI) data

Mature sequence suffixes (“-3p/-5p”) were removed from miRNA names in[46] dataset and names were matched with our miRNA zonation data, after merging miRNAs with duplicate names. Pericentral miRNAs were defined as those with COM ≤ 4.5 and Kruskal-Wallis FDR ≤ 0.2, whereas periportal miRNAs had COM > 4.5 and Kruskal-Wallis FDR ≤ 0.2.

Wilcoxon's rank-sum test was calculated for the ratios log2(treatment/control) of all detected pericentral miRNAs in the plasma versus in the liver.

Analysis of The Cancer Genome Atlas (TCGA) hepatocellular carcinoma (LIHC) data

TCGA-LIHC data (Level 3 miRNA- and mRNA-Seq datasets, not RSEM-normalized) were downloaded using the RTCGA package (https://rtcga.github.io/RTCGA/). In order to match between our microarray miRNA nomenclature, which can inform from which mature miRNA the signal came from (i.e. there are "-3p/-5p" suffixes to the miRNA names), and the RNA-sequencing data which does not have this specificity, names and expression values were merged between degenerate miRNA names. Specifically, 3p/5p suffixes and genomic locus variants (indicated by additional digits after the canonical miRNAnumber) were removed from miRNA names, and the expression values of miRNAs with the resulting identical name were summed over. The resulting TCGA data included values of 1046 miRNA over 372 tumor samples and 50 normal samples. For each miRNA, we computed the log2 ratio of the median expression levels in the tumor samples and the normal samples and examined the Spearman correlations of the log2 ratios and the zonation profile COM for the miRNAs that were included in our spatial sorting study. In order to examine the magnitude of fold change in miRNA expression independently of Wnt pathway mutations, we stratified TCGA data by patients' mutation state and removed from the analysis all patients with mutations in at least one of the genes APC, CTNNB1 and all FZD genes (FZD1-FZD10).

MiRNA-target network construction, randomized networks and genes-miRNA anti-correlation

All miRNA-target interaction predictions were downloaded from TargetScanMouse v7.2[33] (data released 8/2018, downloaded 24/10/18), including conserved and non-conserved sites. Predicted edges were filtered for only liver-expressed miRs, annotated "high confidence" in miRBase v22, weighted context++ score percentile ≥ 95 and genes expressed with maximum fraction (over gates) of total transcriptome ≥ $4\text{x}10^{-6}$). The resulting network included 33,672 interactions between 131 miRNAs and 6,650 genes. For each gene g we constructed the cumulative expression profile $M_g(z)$ of all miRNAs $\mu_i(z)$, $i \in \{1,2,\ldots,N_g\}, z = \{1,\ldots 8\}$ predicted to target it:

$$M_g(z) = \sum_{i=1}^{N_g} \mu_i(z) \quad \text{(Equation 2)}$$

and calculated the Spearman correlation between the expression profile $X_g(z)$ of each gene g and $M_g(z)$. For the network randomization procedure, we only included highly-expressed genes (max expression ≥ 10^{-4}), and genes that are predicted to be regulated by a substantial fraction of the miRNA transcriptome (mean expression of the cumulative miRNA profile ≥ 10^{-3}). This network included 588 genes regulated by 131 miRNAs with 3,502 interactions. We then created 1,000 networks with randomized edge assignment using mfinder[74] with the command *mfinder -r 1000 -ornet -nsr 10*. We took into account miRNAs that regulate the same target genes at multiple sites, and for the purpose of network randomization, these were considered as separate edges by creating "virtual" miRNA nodes that were collapsed back to the original miRNA after randomization. For each randomized network, we calculated again the cumulative miRNA profile for each of the 588 genes and the corresponding Spearman correlation. We then calculated for each gene the fraction of randomized networks in which the anti-correlation of the gene and the original predicted cumulative miRNA expression profiles is smaller than the anti-correlation of the gene with the cumulative profiles generated with the randomized networks, generating an empirical p-value p. We manually corrected genes with $p = 0$ to $p \rightarrow p' = 1/N$, with $N = 1{,}000$ the number of networks generated. FDR values using the Benjamini-Hochberg procedure were calculated for all p-values and genes with FDR ≤ 0.2 were deemed "significant" (Supplementary Table 8).

Regulation of Wnt pathway components

We examined all edges in our miRNA-target network that included genes which are involved in Wnt signaling transduction[75], and that were anti-correlated with individual miRNAs regulating them with a Spearman coefficient of -0.5 or less. The genes were Apc, Axin2, Ctnnb1, Ctnnbip1, Dvl1/2, Fzd1-10, Gsk3, Lgr4/5/6, Lrp5/6, Rnf43, Tcf7, Tcf7l1/2 and Znrf3.

Network visualization

The miRNA-Wnt pathway component network was visualized using Cytoscape v3.7[76]. All detected Wnt pathway components with miRNAs predicted to regulate them (see "miR-target network construction"), and the Spearman correlations between them, were used as input.

Supplementary Material

Refer to Web version on PubMed Central for supplementary material.

Acknowledgements

We thank Efrat Hagai and the Flow Cytometry Unit (Weizmann Institute of Science) for the FACS technical support; Dr. Tamar Ziv and the Smoler Proteomics Center (Technion) for performing the LC-MS/MS and analyzing the results; Dr. David Pilzer and the Genomic Technologies Unit (Weizmann Institute of Science) for performing the miRNA microarray measurements. We thank all members of the lab for valuable comments. S.I. is supported by the Henry Chanoch Krenter Institute for Biomedical Imaging and Genomics, The Leir Charitable Foundations, Richard Jakubskind Laboratory of Systems Biology, Cymerman-Jakubskind Prize, The Lord Sieff of Brimpton Memorial Fund, The Wolfson Family Charitable Trust, The Edmond de Rothschild Foundations, the I-CORE program of the Planning and Budgeting Committee and the Israel Science Foundation (grants 1902/12 and 1796/12), the Israel Science Foundation grant No. 1486/16, the Broad Institute-Israel Science Foundation grant No. 2615/18 the European Research Council (ERC) under the European Union's Horizon 2020 research and innovation programme (grant agreement No 768956), the Bert L. and N. Kuggie Vallee Foundation and the Howard Hughes Medical Institute (HHMI) international research scholar award.

Data availability

RNA sequencing data that support the findings of this study have been deposited in NCBI Sequence Read Archive (SRA) with the BioProject accession code PRJNA556572, and the SRA identifiers SAMN12360372- SAMN12360382. Supplementary Table 2 summarizes the UMI counts per million for each sample. Supplementary Table 11 summarizes the zUMI barcodes used per each sample and the corresponding zUMI settings.

LC-MS/MS proteomic data was uploaded to ProteomeXchange via the PRIDE database, with the project identifier PXD014512. Processed data can be found in Supplementary Table 3.

MiRNA microarray data have been deposited in NCBI Gene Expression Omnibus (GEO) with the primary accession code GSE134827. Supplementary Table 6 summarizes processed miRNA data.

Code availability

Code used to generate the processed data and figures is available upon request.

References

1. Hoehme S, et al. Prediction and validation of cell alignment along microvessels as order principle to restore tissue architecture in liver regeneration. Proc Natl Acad Sci U S A. 2010; 107:10371. [PubMed: 20484673]
2. Wang B, Zhao L, Fish M, Logan CY, Nusse R. Self-renewing diploid Axin2+ cells fuel homeostatic renewal of the liver. Nature. 2015; 524:180–185. [PubMed: 26245375]
3. Colnot, S, Perret, C. Liver ZonationMolecular Pathology of Liver Diseases. Springer; Boston, MA: 2011. 7–16.
4. Odom DT, et al. Control of Pancreas and Liver Gene Expression by HNF Transcription Factors. Science. 2004; 303:1378–1381. [PubMed: 14988562]
5. Halpern KB, et al. Single-cell spatial reconstruction reveals global division of labour in the mammalian liver. Nature. 2017; 542:352. [PubMed: 28166538]
6. Lindros KO, Penttilä KE. Digitonin-collagenase perfusion for efficient separation of periportal or perivenous hepatocytes. Biochem J. 1985; 228:757–760. [PubMed: 2992454]
7. Quistorff B, Grunnet N, Cornell NW. Digitonin perfusion of rat liver. A new approach in the study of intra-acinar and intracellular compartmentation in the liver. Biochem J. 1985; 226:289–297. [PubMed: 3977871]
8. Budnik B, Levy E, Harmange G, Slavov N. Mass-spectrometry of single mammalian cells quantifies proteome heterogeneity during cell differentiation. bioRxiv. 2018; doi: 10.1101/102681
9. Buenrostro JD, et al. Single-cell chromatin accessibility reveals principles of regulatory variation. Nature. 2015; 523:486. [PubMed: 26083756]
10. Doi Y, et al. Development of complementary expression patterns of E- and N-cadherin in the mouse liver. Hepatol Res. 2007; 37:230–237. [PubMed: 17362306]
11. Halpern KB, et al. Paired-cell sequencing enables spatial gene expression mapping of liver endothelial cells. Nat Biotechnol. 2018; 36:962. [PubMed: 30222169]
12. Azimifar SB, Nagaraj N, Cox J, Mann M. Cell-Type-Resolved Quantitative Proteomics of Murine Liver. Cell Metab. 2014; 20:1076–1087. [PubMed: 25470552]
13. Bernhardt, J, Funke, S, Hecker, M, Siebourg, J. Visualizing Gene Expression Data via Voronoi Treemaps. IEEE; 2009. 233–241.
14. Liebermeister W, et al. Visual account of protein investment in cellular functions. Proc Natl Acad Sci. 2014; 111:8488–8493. [PubMed: 24889604]
15. Otto A, et al. Systems-wide temporal proteomic profiling in glucose-starved *Bacillus subtilis* . Nat Commun. 2010; 1:137. [PubMed: 21266987]
16. Schwanhäusser B, et al. Global quantification of mammalian gene expression control. Nature. 2011; 473:337. [PubMed: 21593866]
17. Torre C, Perret C, Colnot S. Molecular Determinants of Liver Zonation. Prog Mol Biol Transl Sci. 2010; 97:127–150. [PubMed: 21074732]
18. Stanulović VS, et al. Hepatic HNF4α deficiency induces periportal expression of glutamine synthetase and other pericentral enzymes. Hepatology. 2007; 45:433–444. [PubMed: 17256722]

19. Colletti M, et al. Convergence of Wnt Signaling on the HNF4α-Driven Transcription in Controlling Liver Zonation. Gastroenterology. 2009; 137:660–672. [PubMed: 19454287]
20. Brosch M, et al. Epigenomic map of human liver reveals principles of zonated morphogenic and metabolic control. Nat Commun. 2018; 9:4150. [PubMed: 30297808]
21. Holloway MG, Miles GD, Dombkowski AA, Waxman DJ. Liver-specific hepatocyte nuclear factor-4alpha deficiency: greater impact on gene expression in male than in female mouse liver. Mol Endocrinol Baltim Md. 2008; 22:1274–1286.
22. Guo H, Ingolia NT, Weissman JS, Bartel DP. Mammalian microRNAs predominantly act to decrease target mRNA levels. Nature. 2010; 466:835. [PubMed: 20703300]
23. Lagos-Quintana M, et al. Identification of Tissue-Specific MicroRNAs from Mouse. Curr Biol. 2002; 12:735–739. [PubMed: 12007417]
24. Kota J, et al. Therapeutic microRNA Delivery Suppresses Tumorigenesis in a Murine Liver Cancer Model. Cell. 2009; 137:1005–1017. [PubMed: 19524505]
25. Sekine S, Ogawa R, Mcmanus MT, Kanai Y, Hebrok M. Dicer is required for proper liver zonation. J Pathol. 2009; 219:365–372. [PubMed: 19718708]
26. Arvey A, Larsson E, Sander C, Leslie CS, Marks DS. Target mRNA abundance dilutes microRNA and siRNA activity. Mol Syst Biol. 2010; 6:363. [PubMed: 20404830]
27. Kozomara A, Griffiths-Jones S. miRBase: annotating high confidence microRNAs using deep sequencing data. Nucleic Acids Res. 2014; 42:D68–D73. [PubMed: 24275495]
28. Bissels U, et al. Absolute quantification of microRNAs by using a universal reference. RNA.
29. Tsai W-C. et al. MicroRNA-122 plays a critical role in liver homeostasis and hepatocarcinogenesis. J Clin Invest. 2012; 122:2884–2897. [PubMed: 22820290]
30. Li W, Dai H, Ou Q, Zuo G, Liu C. Overexpression of microRNA-30a-5p inhibits liver cancer cell proliferation and induces apoptosis by targeting MTDH/PTEN/AKT pathway. Tumor Biol. 2016; 37:5885–5895.
31. Kornfeld J-W. et al. Obesity-induced overexpression of miR-802 impairs glucose metabolism through silencing of Hnf1b. Nature. 2013; 494:111. [PubMed: 23389544]
32. Trajkovski M, et al. MicroRNAs 103 and 107 regulate insulin sensitivity. Nature. 2011; 474:649–653. [PubMed: 21654750]
33. Agarwal V, Bell GW, Nam J-W, Bartel DP. Predicting effective microRNA target sites in mammalian mRNAs. eLife. 2015; 4
34. Benhamouche S, et al. Apc Tumor Suppressor Gene Is the “Zonation-Keeper” of Mouse Liver. Dev Cell. 2006; 10:759–770. [PubMed: 16740478]
35. Birchmeier W. Orchestrating Wnt signalling for metabolic liver zonation. Nat Cell Biol. 2016; 18:463. [PubMed: 27117330]
36. Burke ZD, Tosh D. The Wnt/β-catenin pathway: master regulator of liver zonation? BioEssays. 2006; 28:1072–1077. [PubMed: 17041892]
37. Gebhardt R, Hovhannisyan A. Organ patterning in the adult stage: The role of Wnt/β-catenin signaling in liver zonation and beyond. Dev Dyn. 2009; 239:45–55.
38. Thompson MD, Monga SPS. WNT/β-catenin signaling in liver health and disease. Hepatology. 2007; 45:1298–1305. [PubMed: 17464972]
39. Yang J, et al. Beta-catenin signaling in murine liver zonation and regeneration: A Wnt-Wnt situation! Hepatology. 2014; 60:964–976. [PubMed: 24700412]
40. Planas-Paz L, et al. The RSPO–LGR4/5–ZNRF3/RNF43 module controls liver zonation and size. Nat Cell Biol. 2016; 18:467–479. [PubMed: 27088858]
41. Preziosi M, Okabe H, Poddar M, Singh S, Monga SP. Endothelial Wnts regulate β-catenin signaling in murine liver zonation and regeneration: A sequel to the Wnt–Wnt situation. Hepatol Commun. 2018; 2:845. [PubMed: 30027142]
42. Rocha AS, et al. The Angiocrine Factor Rspondin3 Is a Key Determinant of Liver Zonation. Cell Rep. 2015; 13:1757–1764. [PubMed: 26655896]
43. Shy BR, et al. Regulation of Tcf7l1 DNA Binding and Protein Stability as Principal Mechanisms of Wnt/β-Catenin Signaling. Cell Rep. 2013; 4:1–9. [PubMed: 23810553]

44. Tago K, et al. Inhibition of Wnt signaling by ICAT, a novel beta-catenin-interacting protein. Genes Dev. 2000; 14:1741–1749. [PubMed: 10898789]
45. Ben-Moshe S, Itzkovitz S. Spatial heterogeneity in the mammalian liver. Nat Rev Gastroenterol Hepatol. 2019; 1doi: 10.1038/s41575-019-0134-x
46. Wang K, et al. Circulating microRNAs, potential biomarkers for drug-induced liver injury. Proc Natl Acad Sci. 2009; 106:4402–4407. [PubMed: 19246379]
47. Zucman-Rossi J, Villanueva A, Nault J-C, Llovet JM. Genetic Landscape and Biomarkers of Hepatocellular Carcinoma. Gastroenterology. 2015; 149:1226–1239.e4. [PubMed: 26099527]
48. Chu A, et al. Large-scale profiling of microRNAs for The Cancer Genome Atlas. Nucleic Acids Res. 2016; 44:e3–e3. [PubMed: 26271990]
49. Moor AE, et al. Spatial Reconstruction of Single Enterocytes Uncovers Broad Zonation along the Intestinal Villus Axis. Cell. 2018; 175(4):1156–1167. [PubMed: 30270040]
50. Park J, et al. Single-cell transcriptomics of the mouse kidney reveals potential cellular targets of kidney disease. Science. 2018; doi: 10.1126/science.aar2131
51. Guder WG, Ross BD. Enzyme distribution along the nephron. Kidney Int. 1984; 26:101–111. [PubMed: 6094907]
52. Xu H, et al. Liver-enriched transcription factors regulate MicroRNA-122 that targets CUTL1 during liver development. Hepatology. 2010; 52:1431–1442. [PubMed: 20842632]
53. Berndt N, Horger MS, Bulik S, Holzhütter H-G. A multiscale modelling approach to assess the impact of metabolic zonation and microperfusion on the hepatic carbohydrate metabolism. PLoS Comput Biol. 2018; 14
54. Godoy P, et al. Recent advances in 2D and 3D in vitro systems using primary hepatocytes, alternative hepatocyte sources and non-parenchymal liver cells and their use in investigating mechanisms of hepatotoxicity, cell signaling and ADME. Arch Toxicol. 2013; 87:1315–1530. [PubMed: 23974980]
55. Holzhütter H-G, Drasdo D, Preusser T, Lippert J, Henney AM. The virtual liver: a multidisciplinary, multilevel challenge for systems biology. Wiley Interdiscip Rev Syst Biol Med. 2012; 4:221–235. [PubMed: 22246674]
56. Jopling CL, Yi M, Lancaster AM, Lemon SM, Sarnow P. Modulation of Hepatitis C Virus RNA Abundance by a Liver-Specific MicroRNA. Science. 2005; 309:1577–1581. [PubMed: 16141076]
57. Roderburg C, et al. Micro-RNA profiling reveals a role for miR-29 in human and murine liver fibrosis. Hepatology. 2011; 53:209–218. [PubMed: 20890893]
58. Mitchell PS, et al. Circulating microRNAs as stable blood-based markers for cancer detection. Proc Natl Acad Sci. 2008; 105:10513–10518. [PubMed: 18663219]
59. Farid W, et al. Hepatocyte-derived microRNAs as serum biomarkers of hepatic injury and rejection after liver transplantation. Liver transpl. 2012; 18(3):290–297. [PubMed: 21932376]
60. Dominissini D, et al. Topology of the human and mouse m^6A RNA methylomes revealed by m^6A-seq. Nature. 2012; 485:201. [PubMed: 22575960]
61. Hirayama A, et al. Quantitative Metabolome Profiling of Colon and Stomach Cancer Microenvironment by Capillary Electrophoresis Time-of-Flight Mass Spectrometry. Cancer Res. 2009; 69:4918–4925. [PubMed: 19458066]
62. Llufrio EM, Wang L, Naser FJ, Patti GJ. Sorting cells alters their redox state and cellular metabolome. Redox Biol. 2018; 16:381–387. [PubMed: 29627745]
63. Manco R, et al. Reactive cholangiocytes differentiate into proliferative hepatocytes with efficient DNA repair in mice with chronic liver injury. J Hepatol. 2019; 70:1180–1191. [PubMed: 30794890]
64. Mederacke I, Dapito DH, Affò S, Uchinami H, Schwabe RF. High-yield and high-purity isolation of hepatic stellate cells from normal and fibrotic mouse livers. Nat Protoc. 2015; 10:305. [PubMed: 25612230]
65. Tanami S, et al. Dynamic zonation of liver polyploidy. Cell Tissue Res. 2017; 368:405–410. [PubMed: 27301446]
66. Bagnoli JW, et al. Sensitive and powerful single-cell RNA sequencing using mcSCRB-seq. Nat Commun. 2018; 9:2937. [PubMed: 30050112]

67. Parekh S, Ziegenhain C, Vieth B, Enard W, Hellmann I. zUMIs - A fast and flexible pipeline to process RNA sequencing data with UMIs. GigaScience. 2018; 7

68. Robinson MD, Oshlack A. A scaling normalization method for differential expression analysis of RNA-seq data. Genome Biol. 2010; 11:R25. [PubMed: 20196867]

69. Robinson MD, McCarthy DJ, Smyth GK. edgeR: a Bioconductor package for differential expression analysis of digital gene expression data. Bioinformatics. 2010; 26:139–140. [PubMed: 19910308]

70. Cox J, Mann M. MaxQuant enables high peptide identification rates, individualized p.p.b.-range mass accuracies and proteome-wide protein quantification. Nat Biotechnol. 2008; 26:1367. [PubMed: 19029910]

71. Li B, et al. Adult Mouse Liver Contains Two Distinct Populations of Cholangiocytes. Stem Cell Rep. 2017; 9:478–489.

72. Newman AM, et al. Robust enumeration of cell subsets from tissue expression profiles. Nat Methods. 2015; 12:453–457. [PubMed: 25822800]

73. Kanehisa M, Goto S. KEGG: Kyoto Encyclopedia of Genes and Genomes. Nucleic Acids Res. 2000; 28:27–30. [PubMed: 10592173]

74. Milo R, et al. Network Motifs: Simple Building Blocks of Complex Networks. Science. 2002; 298:824. [PubMed: 12399590]

75. Nusse R, Clevers H. Wnt/β-Catenin Signaling, Disease, and Emerging Therapeutic Modalities. Cell. 2017; 169:985–999. [PubMed: 28575679]

76. Shannon P, et al. Cytoscape: a software environment for integrated models of biomolecular interaction networks. Genome Res. 2003; 13:2498–2504. [PubMed: 14597658]

77. Krützfeldt J, et al. Silencing of microRNAs in vivo with ‘antagomirs’. Nature. 2005; 438:685. [PubMed: 16258535]

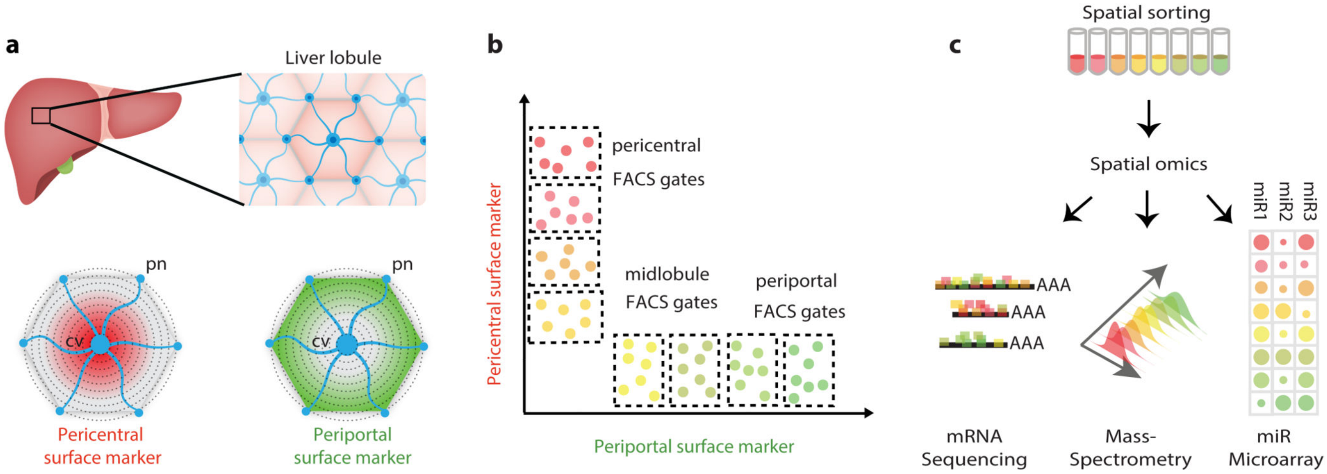

Fig. 1. Spatial sorting approach for isolating large amounts of hepatocytes from distinct layers with high resolution.

a, Identification of zonated surface markers. cv – central vein. pn – portal node. **b**, Fluorescence-activated cell sorting (FACS) enables defining gates that enrich for zonated hepatocytes according to their surface marker expression. **c**, Spatially-sorted hepatocytes can be measured using multiple assays that require large input material, such as RNA-seq, Mass spectrometry and miRNA microarray applied in the current study.

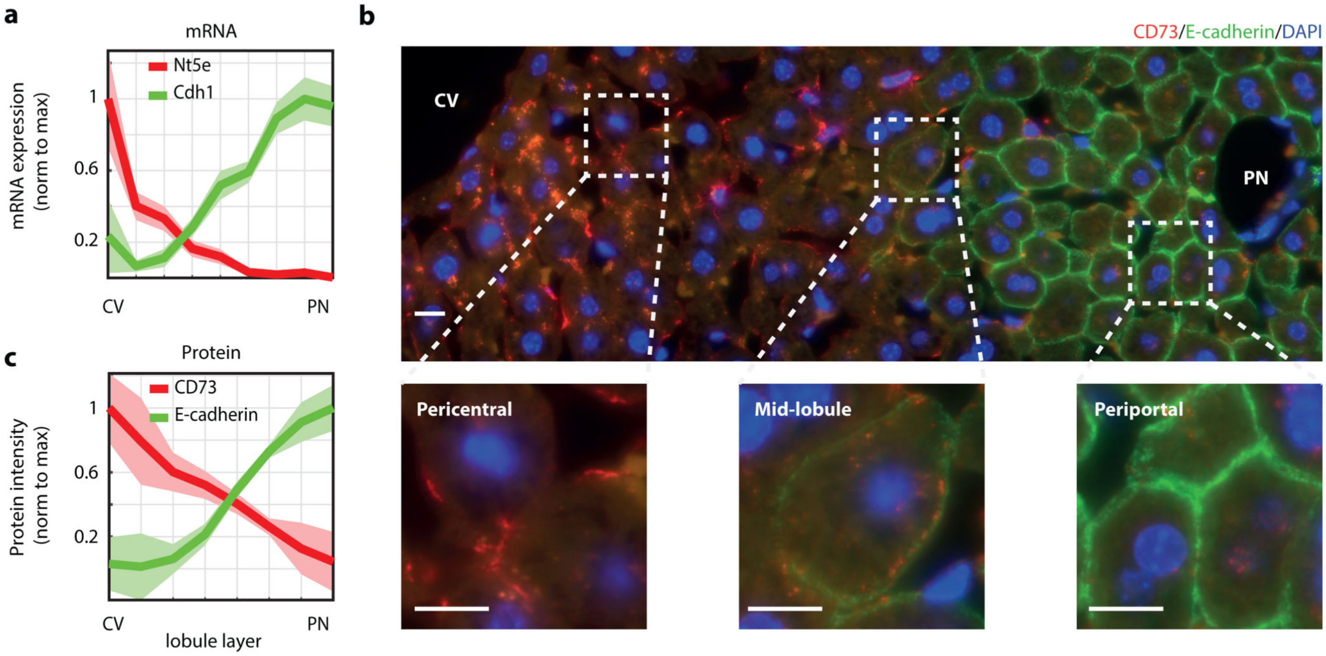

Fig. 2. CD73 and E-cadherin are inversely zonated surface markers.

a, CD73, encoded by Nt5e, and E-cadherin, encoded by Cdh1, are surface markers that are zonated at the mRNA level. Data taken from [5], n=1415 cells from 3 mice. Lines show sum-normalized mean of all cells, shaded regions are ±SEM. **b,** CD73 and E-cadherin proteins are zonated. Shown is an example of a lobule stained by immunofluorescence with antibodies against CD73 (red) and E-cadherin (green). Blue – DAPI nuclear stain. Scale bar – 10μm. Experiment was prformed independently on 3 different mice. **c,** Quantification of immunofluorescence images (n=8 lobules from three mice). Lines represent the mean of intensity measured in the lobule layer, shaded regions are ±SEM across the eight lobules. CV – central vein, PN – portal node.

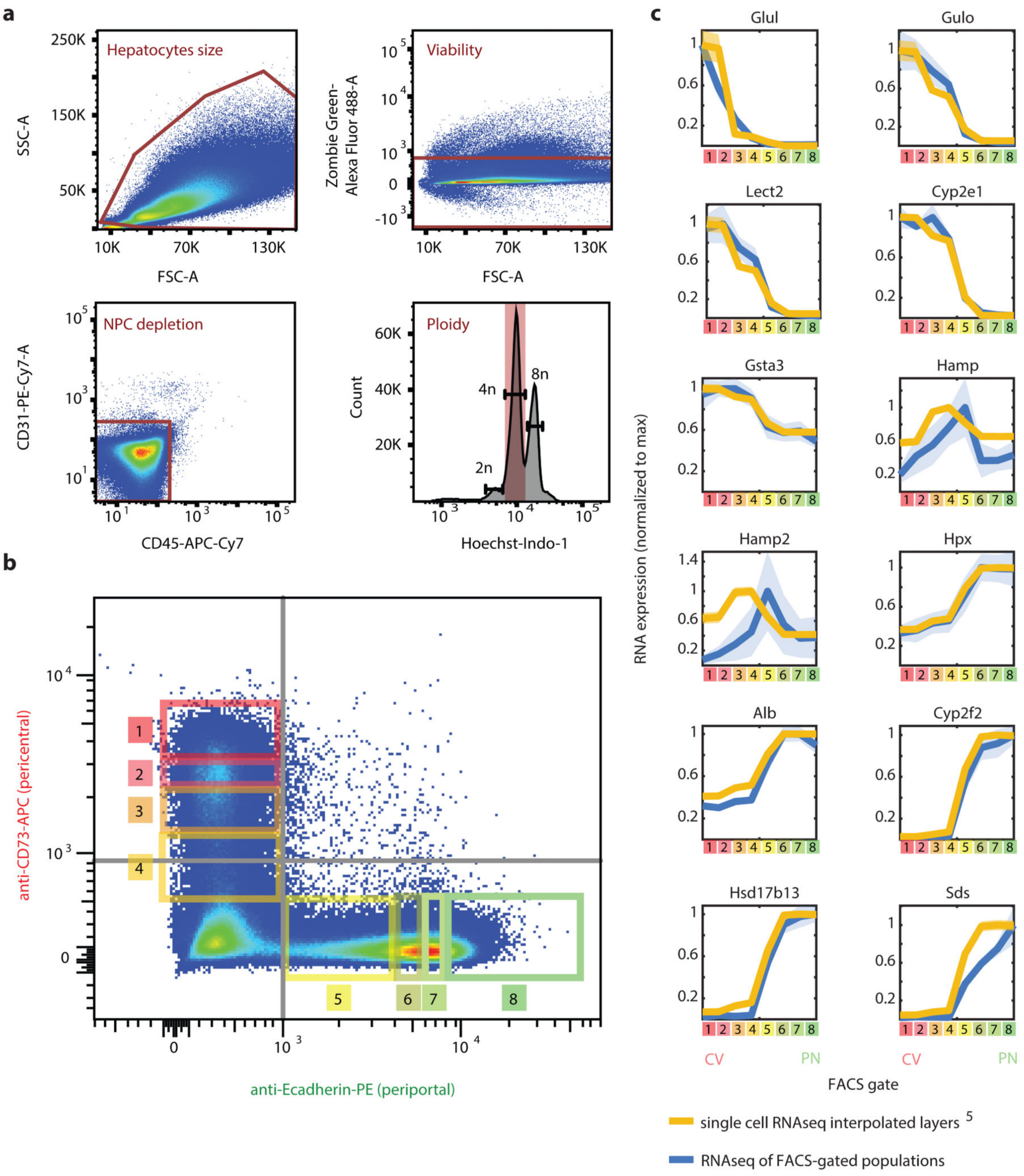

Fig. 3. Spatial sorting reliably captures the different lobule layers.

a, FACS gating strategy. FSC-A and SSC-A were used for hepatocytes size selection. Non-viable cells were filtered out by Zombie Green Viability kit. Staining with CD31 and CD45 antibodies enabled gating-out non-parenchymal cells. Tetraploid hepatocytes were selected based on Hoechst stain. **b**, Distribution of the included cells (40-60% from all events) according to intensities of CD73 and E-cadherin. Grey lines mark the unstained control limits, rectangles and numbers mark the gates used for spatially-sorted populations. Distributions from five independent mice were similar. **c**, Max-normalized expression patterns of selected genes along the different FACS gates in blue (N=5 mice), compared with interpolated max-normalized zonation profiles based on [5] in yellow. Lines are the mean of each FACS gate for the 5 mice (blue) and mean of each interpolated layer for the 1415 cell from 3 mice (yellow). Line patches represent SEM.

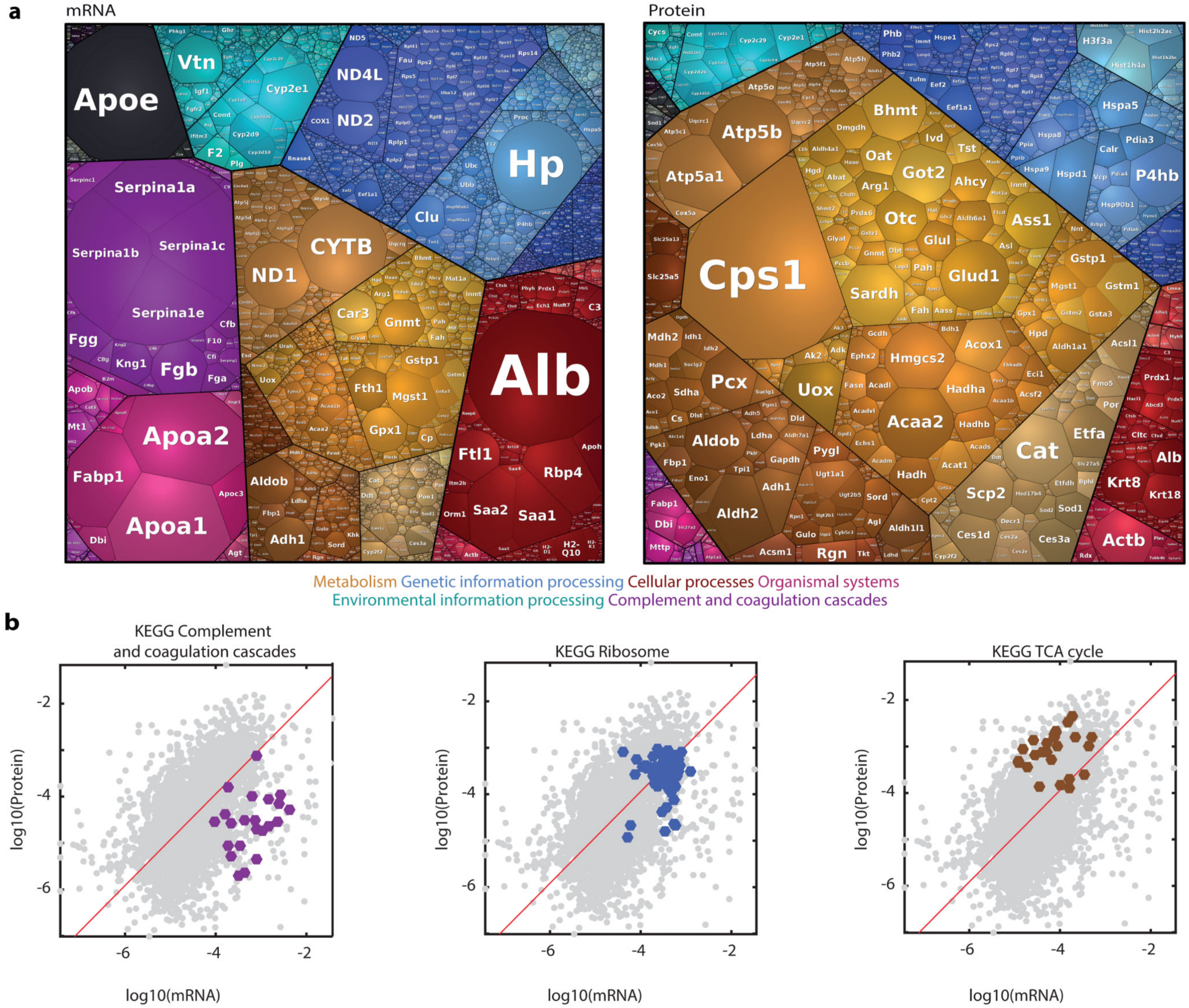

Fig. 4. Correlations between mRNA and protein levels.

a, Proteomaps for visualizing the distributions of the mean mRNA and mean proteins over all FACS gates. Each tile in the map represents a gene, size is proportional to its fraction in the total dataset. Tile colors represent different gene annotations, color-code legend is below the maps. Genes/protein closer on the maps and sharing the same color are closer in function. Visualization was done using https://bionic-vis.biologie.uni-greifswald.de/ [13–15]. Color classification key for selected categories is shown at the bottom. **b**, Gate-averaged mRNA and protein levels are mildly correlated (Spearman's r=0.5). Shown are three KEGG functional classifications with distinct ratios of mRNAS and proteins. Red is a linear regression line. n = 3,051 genes averaged over 5 mice.

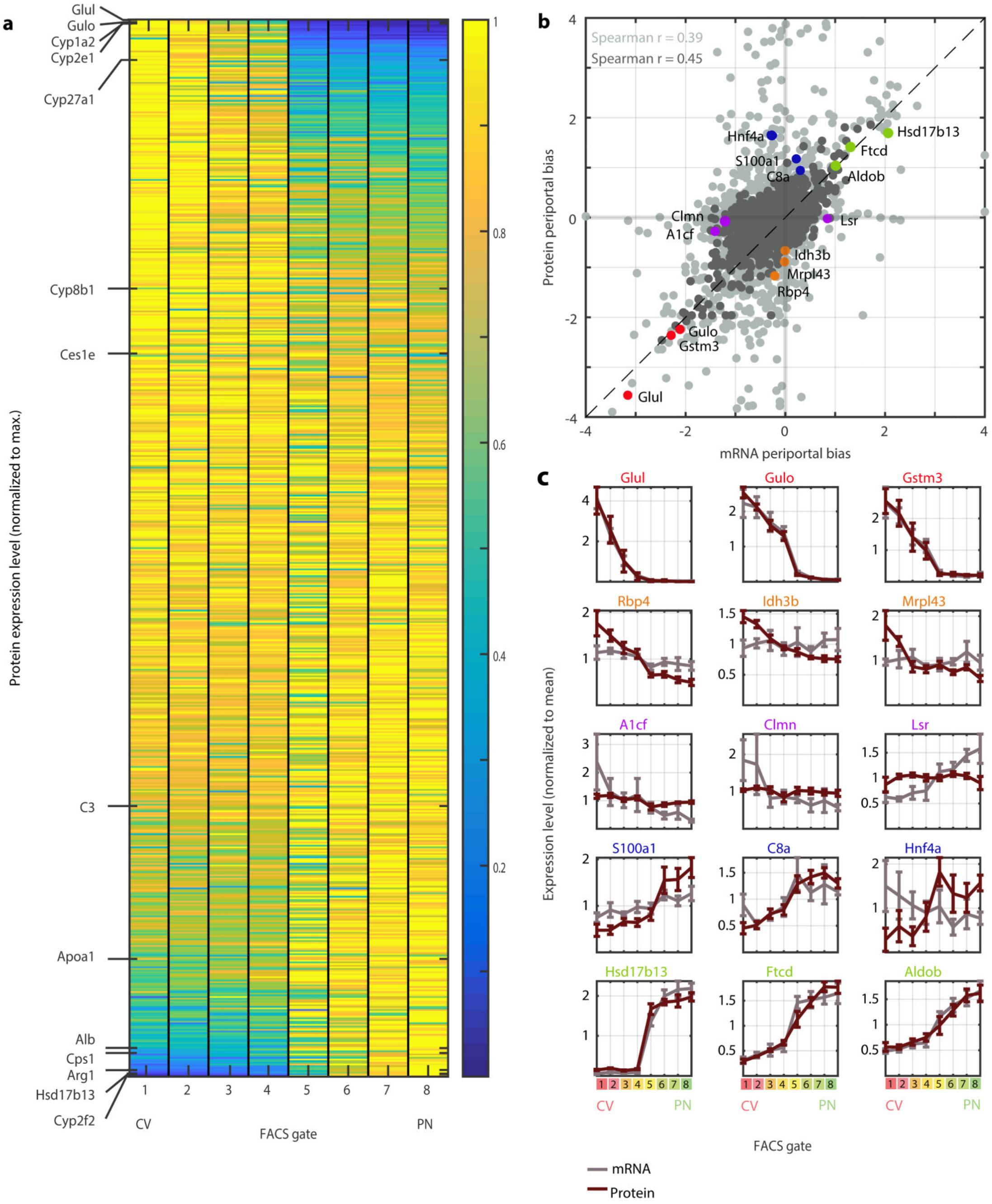

Fig. 5. A spatial atlas of the hepatocyte proteome.

a, Zonation of hepatocyte proteins. Genes are sorted by the zonation profile center of mass. Representative liver proteins are shown on the left, to demonstrate the zonation profiles visualization. Protein levels were normalized to the maximal level across all FACS gates. **b**, Periportal bias in expression of mRNA and proteins, calculated as the difference between the two periportal gates and the two pericentral gates, normalized by the mean expression across all gates. Light grey – all matched mRNA and proteins (n=3,051). Dark grey – mRNA and proteins with minimal expression fraction higher than 10^{-5} in any of the gates for both mRNA and protein (n=1,565). Spearman’s r is indicated for each dataset. Dashed line marks a slope of 1. N=5 mice **c**, Expression profiles of mRNA (grey) and their respective proteins (red). Mean of five mice is plotted. Error bars represent SEM.

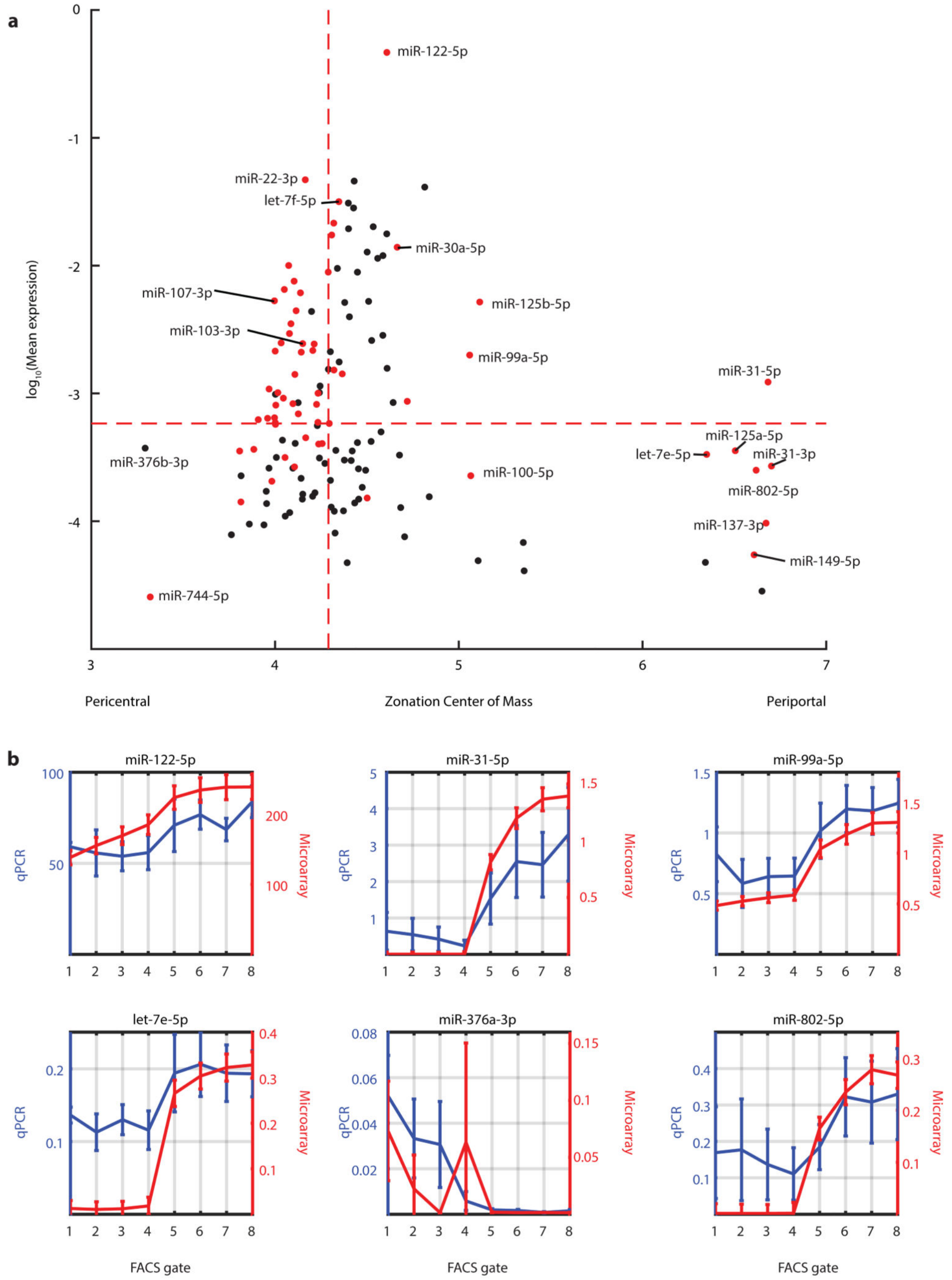

Fig. 6. Zonated expression of hepatocyte miRNAs.

a, Mean expression vs. zonation profile center of mass for all detected high-confidence miRNAs. Selected miRNAs are labelled. Dashed red lines denote the median of each quantity. Red dots are miRNAs that are significantly zonated (two sided Kruskal-Wallis test with following Benjamini-Hochberg FDR ≤ 0.2). N=3 mice. **b**, Validations of hepatocyte miRNA zonation profiles using qRT-PCR. Profiles for both qRT-PCR and microarrays are normalized by expression levels of miR-103-3p (Spearman's r = 0.70±0.24). Lines indicate layer mean over 3 microarry mouse-repeats (red) and layer mean over 3 qPCR mouse-repeats (blur). Error bars indicate SEM. Discrepancies between qRT-PCR and microarray profiles for let-7e-5p, miR-376a and miR-802-5p may be due to limited sensitivity of the microarray at low expression levels. N=3 mice for microarray and for qPCR.

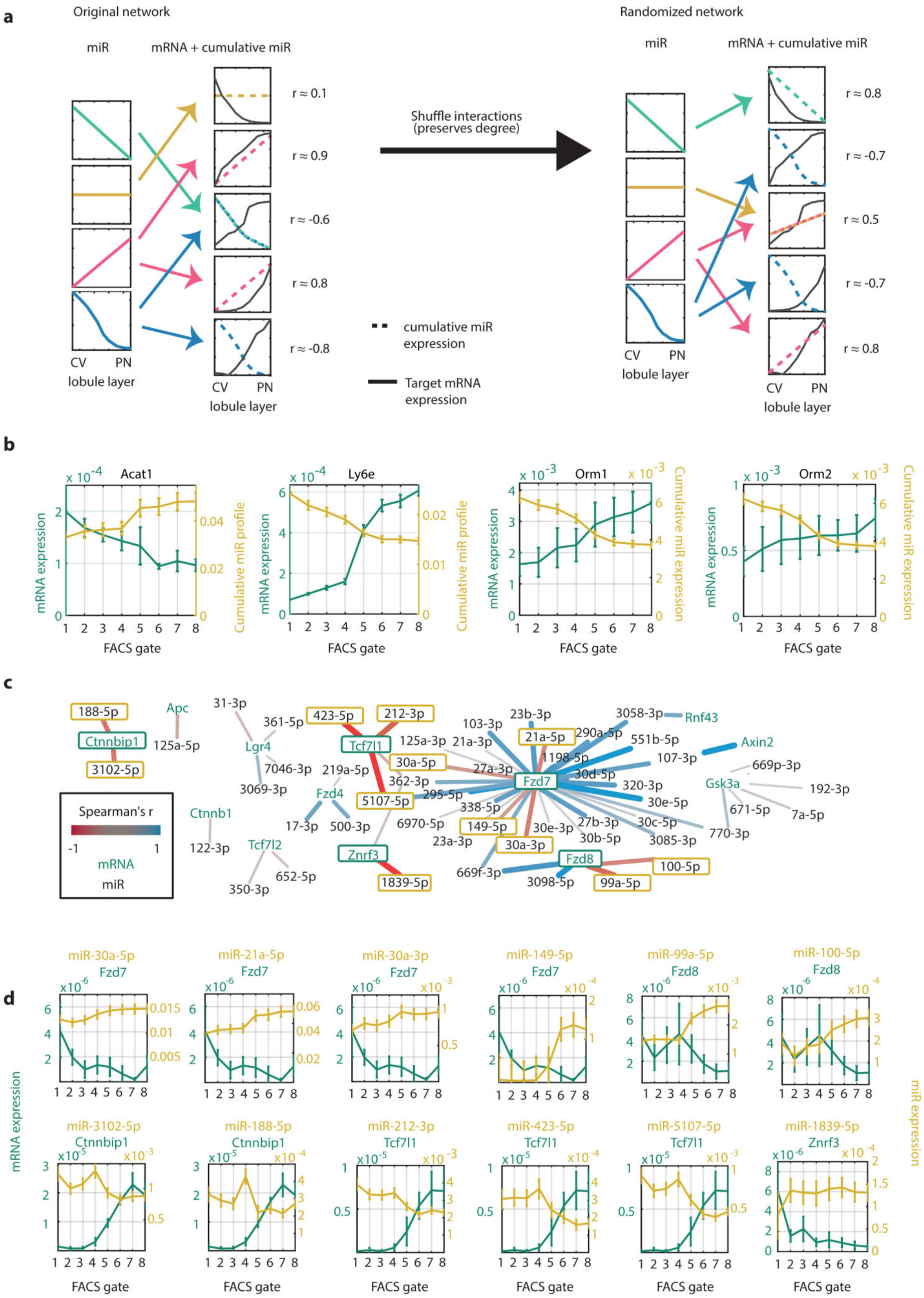

Fig. 7. Network analysis of miRNA-target interactions.

a, Schematic illustration of the algorithm for inferring significant interactions between miRNAs and target genes. **b**, Zonation profiles of selected genes and their significantly anti-correlated cumulative miRNA profiles. Lines represent mean of 5 mice for mRNA (green) and 3 mice for miRNA (yellow). Error bars are SEM. **c**, Regulatory network of hepatocyte-expressed Wnt pathway components and their expressed regulating miRNAs. Edges colored by the correlation between the miRNA and target. Edge weight is proportional to the absolute correlation value. N=3 mice for miRNA dataset, 5 mice for mRNA set. **d**, Selected pairs of miRNAs and regulated Wnt signaling components (outlined in green in Fig. 7c). The transcripts of Ctnnbip1, Fzd8, Tcf7l1 and Znrf3 are anti-correlated with most of their regulating miRs, suggesting that miRNAs have a relatively more important role in regulating these genes' expression in comparison to other genes. Lines represent mean of 5 mice for mRNA (green) and 3 mice for miRNA (yellow). Error bars are SEM.